

Controlling the Excited State and Photosensitizing Property of a 2-(2-Pyridyl)benzo[*b*]thiophene-Based Cationic Iridium Complex through Simple Chemical Modification

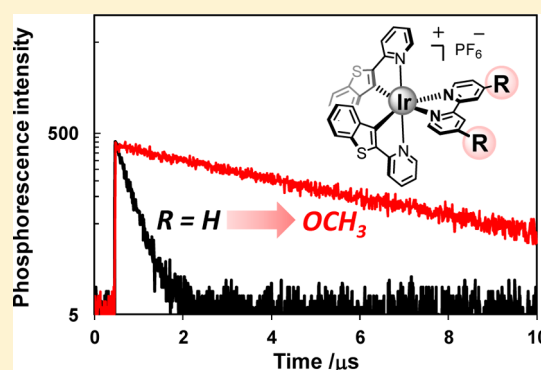
Shin-ya Takizawa,^{*,†} Kengo Shimada,[†] Yoichi Sato,[‡] and Shigeru Murata^{*,†}

[†]Department of Basic Science, Graduate School of Arts and Sciences, The University of Tokyo, 3-8-1 Komaba, Meguro-ku, Tokyo 153-8902, Japan

[‡]Graduate School of Science, The University of Tokyo, 7-3-1 Hongo, Bunkyo-ku, Tokyo 113-0033, Japan

S Supporting Information

ABSTRACT: Bis-cyclometalated cationic iridium (Ir) complexes 1–4 comprising two 2-(2-pyridyl)benzo[*b*]thiophene (btp) ligands and one 2,2'-bipyridyl (bpy) ancillary ligand with different substituents were prepared as new visible light-absorbing sensitizers and examined for their photophysical and electrochemical properties. Complex 1 was prepared as a parent complex without any substituents. Complexes 2–4 contained methyl-, methoxy-, and trifluoromethyl groups at 4,4'-positions on the bpy ancillary ligand. Systematic investigation of these complexes revealed that such a simple chemical modification selectively controls the excited-state lifetime, while the absorption and emission spectral features remain unchanged. Specifically, the phosphorescence lifetimes of complexes 2 and 3 with electron-donating groups ($\tau = 3.50 \mu\text{s}$, $3.90 \mu\text{s}$) were found to be much longer than that of complex 1 ($\tau = 0.273 \mu\text{s}$), and complex 4,



possessing strong electron-withdrawing trifluoromethyl groups, did not exhibit detectable phosphorescence at room temperature. The large differences in excited-state lifetimes of complexes 1–3, as well as the nonemissive character of complex 4, are attributed to a strong influence of the substituents on the ligand field strength. The increased σ -donating ability of the ancillary ligand in complexes 2 and 3 destabilizes a short-lived, nonemissive triplet metal-centered (^3MC) state and increases the energy separation between the ^3MC state and emissive triplet ligand-centered (^3LC) state based on the btp ligand. For complex 4, however, the ^3MC state is close in energy to the ^3LC state because of the decreased σ -donating ability of the ancillary ligand. Additional evidence of the ^3MC state associated with the changeable excited state was also provided via low-temperature phosphorescence measurements and density functional theory calculations. Ir complexes 1–4 were tested as sensitizers in photoinduced electron-transfer reaction of triethanolamine and methylviologen chloride (MVCl_2). As a result, complexes 2 and 3 exhibited much better photosensitizing property compared to complex 1 since their long-lived excited states promoted an oxidative quenching pathway. This study has first demonstrated that simple substitution on the diimine ancillary ligand can control the ^3MC state of the bis-cyclometalated cationic Ir complex to finely tune the excited-state lifetime and photosensitizing property.

INTRODUCTION

Bis-cyclometalated cationic iridium (Ir) complexes have gained a growing interest in the fields of light-emitting electrochemical cells (LECs)¹ and bioimaging.² These applications utilize phosphorescence from the Ir complexes, which is observable at room temperature, as the strong spin–orbit coupling of the heavy Ir metal allows efficient intersystem crossing (ISC) from the singlet excited state to the triplet excited state. In addition, rational design and selection of the cyclometalating ligand and ancillary ligand provide an opportunity to control the photophysical, electrochemical, and steric properties of the Ir complexes.³

During the past decade, attention has been partly directed to evaluation of these complexes as sensitizers in a number of ways including photoinduced hydrogen (H_2) generation from water, singlet oxygen generation,⁴ free radical photopolymeriza-

tions,⁵ and organic synthesis.⁶ In particular, photoinduced H_2 generation is the subject of intense research focused on the development of alternative energy sources as a response to the continued combustion of fossil fuels as well as increasing human energy consumption. Recent advances are strongly influenced by pioneering works of Bernhard's group that reported sensitizers based on iridium(III) bis(2-phenylpyridinato-*N,C*2')-2,2'-bipyridine hexafluorophosphate $[\text{Ir}(\text{ppy})_2(\text{bpy})]\text{PF}_6$ and its derivatives.⁷ For instance, photoinduced H_2 generation with the Ir sensitizers has been extensively investigated by several research groups using different catalytic systems.⁸ Nevertheless, a challenging task remains that new useful Ir sensitizers for effective solar energy utilization need to

Received: November 6, 2013

Published: February 26, 2014

be developed, since the major obstacle in the application of the present complexes appears to be the limited availability of Ir sensitizers that have strong absorption in the visible spectral region.⁹ In addition to the visible light-absorbing property, a long excited-state lifetime is required for favorable electron-transfer to occur between the excited sensitizer and an electron donor or acceptor. Equally important is high photochemical stability of the sensitizers to construct robust visible light-driven H₂ generation systems.

Bearing this context in mind, we set out to synthesize bicyclic metalated cationic Ir complexes containing 2-(2-pyridyl)-benzo[*b*]thiophene (btp) ligands as new sensitizers. Among the representative Ir complexes with the btp ligands is electro-neutral bis[2-(benzo[*b*]thiophen-2-yl)pyridinato-*N,C*^{3'}]iridium(acetylacetonate), Ir(btp)₂(acac),¹⁰ which has a larger molar extinction coefficient in the visible region than that of [Ir(ppy)₂(bpy)]PF₆. Ir(btp)₂(acac) has been frequently used as a red-emitting material in organic light-emitting devices (OLEDs) due to its moderate phosphorescence quantum yield.¹¹ More recently, some research groups reported corresponding cationic complexes having the 1,10-phenanthroline ancillary ligand in sensing applications.¹² Cationic Ir complexes are also beneficial in terms of high photochemical stability,^{4a} availability of many different diimine ancillary ligands for the desired photophysical properties, and solubility in water.¹³ Here we report the first preparation and fundamental photophysical study of cationic Ir complexes 1–4 coordinated with 2,2'-bipyridyl (bpy) and its derivatives as an ancillary ligand (Chart 1). Since any detailed photochemical behavior of

unexpectedly revealed that such a simple chemical modification selectively controls the excited-state lifetime without any appreciable changes in absorption and emission spectral features and leads to improved photosensitizing properties. In this Article, we rationalize the reason behind the changeable excited state and photosensitizing properties of the btp-based Ir complex depending on the substituent groups on the ancillary ligand. Electrochemical measurements and theoretical calculations were also performed to offer an insight into the frontier orbital distributions and their energy levels.

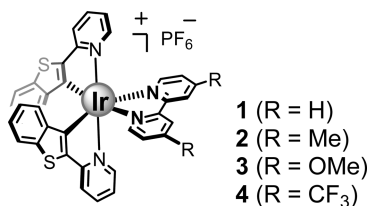
RESULTS AND DISCUSSION

Synthesis. As outlined in Scheme 1, complexes 1–4 were successfully synthesized by a reaction of di- μ -chloro-bridged Ir(III) dimer 5 with the corresponding bpy analogues, followed by anion metathesis reaction of the chloride salts with ammonium hexafluorophosphate (NH₄PF₆). Dimer 5 was prepared by a standard method previously reported in literature,^{10a} yet insolubility in common deuterated solvents, except for DMSO-*d*₆, precluded its characterization by ¹H NMR spectroscopy. Although dimer 5 was soluble well in DMSO-*d*₆, we could not exclude the possibility that DMSO might cause cleavage of the chloro bridge to form [Ir(btp)₂(DMSO)₂]Cl.¹⁴ Thus, dimer 5 was used for the next reaction without further purification and characterization. Reaction of dimer 5 with each bpy ligand proceeded well in hot ethylene glycol, and the subsequent anion metathesis reaction with NH₄PF₆ led to complexes 1–4. Although we were unable to obtain X-ray quality crystals, complexes 1–4 were fully characterized by ¹H NMR, mass spectrometry, and elemental analysis. Complexes 1–4 are C₂-symmetric, as depicted in Chart 1 and Scheme 1, because their ¹H NMR spectra showed one set of proton signals corresponding to the btp ligand and the pyridyl moiety of the bpy ancillary ligand.

Photophysical Properties at Room Temperature.

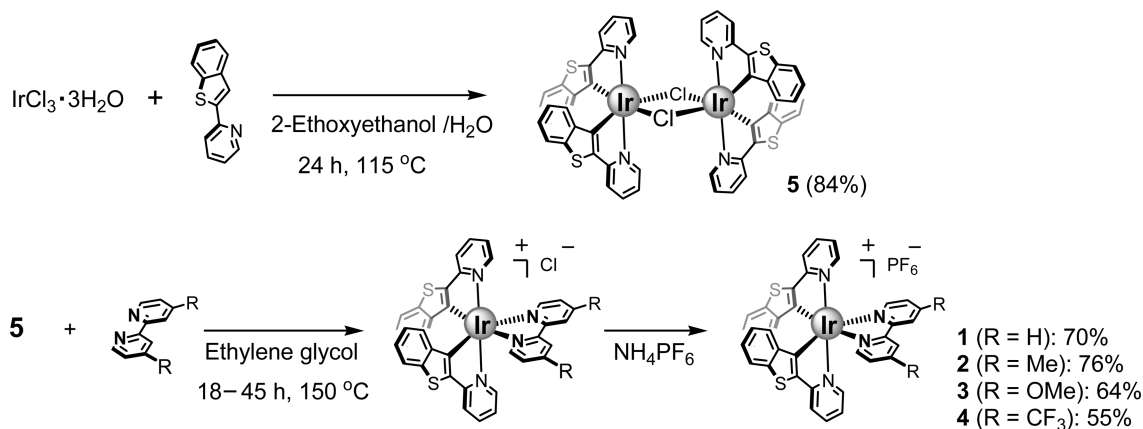
Ultraviolet–visible (UV–vis) absorption spectra of complexes 1–4 were recorded in acetonitrile (CH₃CN) at room temperature, as shown in Figure 1. The absorption maxima together with molar extinction coefficients are listed in Table 1. All these complexes exhibited intense absorptions dominated by the π – π^* transitions of the btp and bpy moieties, with maxima between 250 and 350 nm. In addition, the complexes showed less intense absorption bands centered around 428–437 nm. The spectral profiles of complexes 1–4 resemble each other in the latter low-energy region, but it was found that the

Chart 1. Chemical Structure of Ir Complexes 1–4



this type of cationic Ir complex bearing the bpy ligand has not yet been evaluated, the main goal of our study was to ascertain whether electron-donating or withdrawing substituents on the bpy ligand affect the triplet energy and absorption spectrum of the parent complex 1. However, our systematic investigation

Scheme 1. Synthetic Route of Ir Complexes 1–4



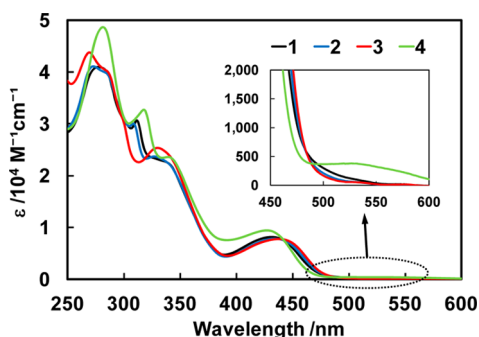


Figure 1. UV-vis absorption spectra of complexes 1–4 in CH₃CN. (inset) Expanded view for the low-energy spectral region.

electron-donating methyl (Me) and methoxy (OMe) groups on the bpy ligand slightly redshift the absorption maximum, while the presence of the electron-withdrawing trifluoromethyl (CF₃) group results in hypsochromic shift of 3 nm (162 cm⁻¹). Such absorptions in the visible region, not present in the free btp and bpy ligands (Supporting Information, Figure S1) and generated by coordination of btp to the Ir metal ion, may be attributed to electronic transitions that are closely related to the metal center. These are spin-allowed singlet metal–ligand-to-ligand charge transfer (¹MLLCT) transitions associated mainly with the btp ligand. Note that previously mentioned Ir(btp)₂(acac), where the diimine ancillary ligand is replaced with the nonchromophoric acetylacetonate, was reported to exhibit a similar visible-light absorption band (484 nm, $\epsilon = 6300 \text{ M}^{-1} \text{ cm}^{-1}$).^{10b} This proof of Ir(btp)₂(acac) complementarily indicates that participation of the btp ligand is more significant in the visible spectral region rather than that of the bpy ancillary ligand. Unlike complexes 1–3, complex 4 showed another very weak absorption band around 530 nm. This might be understood as a result of an insignificant contribution of the ¹MLLCT transition related to the bpy ligand; the strong electron-withdrawing CF₃ groups are thought to lower the energy level of the LUMO localized on the bpy moiety and may visualize the lowest-energy component of the electronic transitions.

Emission spectra of complexes 1–3 were measured in deaerated CH₃CN at room temperature (Figure 2). As presented in Figure 2, complexes 1–3 displayed vibronically structured phosphorescence with almost identical spectral shape and emission maxima. The photoluminescence excitation spectra of complexes 1–3 closely matched the absorption spectra (Supporting Information, Figures S2–S4), illustrating that phosphorescence shown in Figure 2 unarguably comes from the target Ir complexes. It is generally accepted that structured emission originates from an excited state predominantly with ligand-centered (LC) character on the cyclo-

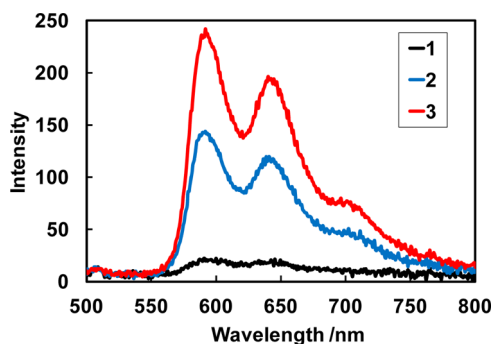


Figure 2. Emission spectra of complexes 1–3 excited at 300 nm (9 μM in CH₃CN at room temperature).

metalating ligands, whereas broad and featureless emission has a character of high charge-transfer component such as ³MLCT and triplet ligand-to-ligand charge transfer (³LLCT).^{10a,15} Accordingly, the emissive excited states of complexes 1–3 consist mainly of the ³LC state on the btp ligand. This is also supported by the fact that the substitution on the bpy ligand does not have a significant effect on the emission maxima. Despite the similarity in the emission spectral profiles of complexes 1–3, an interesting aspect was found based on other phosphorescence properties: the emission quantum yields of complexes 2 and 3 with electron-donating groups were considerably higher than that of complex 1 (see Table 1). In sharp contrast, complex 4 with the CF₃ groups was not emissive at room temperature. These results are particularly intriguing, because a fairly simple modification of the bpy ancillary ligand seems to have a dramatic impact on the triplet excited-state dynamics even though the emissive triplet state remains unchanged in energy.

To facilitate the investigation of this photophysical behavior, phosphorescence lifetimes were measured for complexes 1–3 in deaerated CH₃CN at room temperature. Figure 3 depicts their phosphorescence decay profiles that evidently indicate remarkably longer lifetimes of complexes 2 and 3 compared to that of complex 1. Each decay profile was well-fitted to a single exponential function, and the phosphorescence lifetimes of complexes 1, 2, and 3 were determined to be 0.273 μs , 3.50 μs , and 3.90 μs , respectively. Although the lifetime of complex 1 is relatively short, the lifetime data prove the phosphorescent nature of complexes 1–3. Additionally, Table 1 includes radiative (k_r) and nonradiative (k_{nr}) rate constants, determined using eqs 1 and 2, where Φ and τ denote emission quantum yield and phosphorescence lifetime, respectively.

$$k_r = \frac{\Phi}{\tau} \quad (1)$$

Table 1. Photophysical Properties of Complexes 1–4 in CH₃CN at Room Temperature

	λ_{abs} (nm) (ϵ ($10^4 \text{ M}^{-1} \text{ cm}^{-1}$)) ^a	λ_{em} (nm) ^b	Φ ^c	τ (μs) ^d	k_r (s^{-1}) ^e	k_{nr} (s^{-1}) ^f
1	277 (4.09), 312 (3.06), 335 (2.28), 431 (0.813)	590, 645	0.009	0.273	3×10^4	4×10^6
2	273 (4.11), 308 (3.00), 327 (2.37), 435 (0.780)	590, 641, 700	0.064	3.50	1.8×10^4	2.7×10^5
3	270 (4.38), 330 (2.53), 437 (0.774)	592, 642, 699	0.107	3.90	2.74×10^4	2.29×10^5
4	282 (4.86), 318 (3.27), 339 (2.36), 428 (0.94), 527 (0.0380)	— ^g				

^aAbsorption maxima (molar extinction coefficient). ^bPhosphorescence maxima. ^cPhosphorescence quantum yield measured in deaerated CH₃CN. ^dPhosphorescence lifetime measured in deaerated CH₃CN. ^eRadiative rate constant. ^fNonradiative rate constant. ^gThis complex does not exhibit luminescence. Thus, the photophysical values could not be determined.

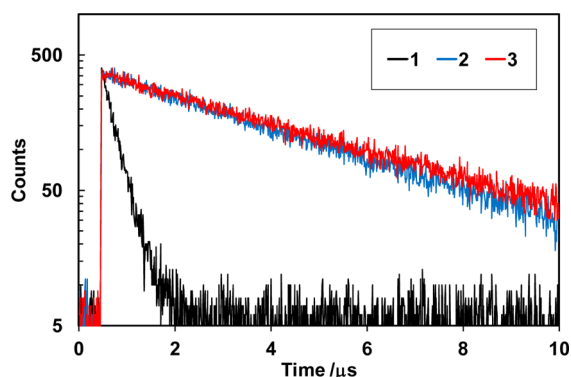
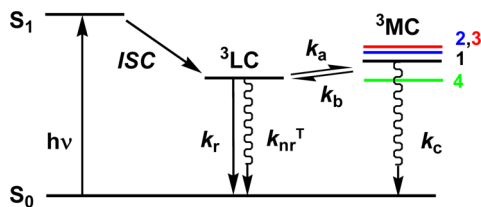


Figure 3. Phosphorescence decay profiles of complexes 1–3 in CH_3CN at room temperature.

$$k_{\text{nr}} = \frac{1 - \Phi}{\tau} = \frac{1}{\tau} - k_{\text{r}} \quad (2)$$

Clearly, from Table 1, the radiative rate constants are relatively invariable, irrespective of the substituents introduced on the bpy ligand. However, the nonradiative rate constant of complex 1 is 15–17 times larger than those of complexes 2 and 3 with electron-donating Me and OMe groups. These combined results lead to the assumption that the excited states of complexes 1–4 may involve thermal population to a triplet metal-centered (^3MC) state, and the electron-donating groups partly suppress the conversion from the emissive triplet excited state (^3LC) to the short-lived, nonemissive ^3MC state. Nevertheless, a large part of the ^3LC state energy seems to be still directed toward the ^3MC state even in complexes 2 and 3, since their phosphorescence quantum yields were determined to be only 6.4% and 10.7%, respectively. On the other hand, the ^3MC state may be populated easily in complex 4 having the electron-withdrawing CF_3 groups. In the present case, the energy-gap law¹⁶ cannot be applied to explain the large k_{nr} value of complex 1 as complexes 1–3 have a common nature of the emitting ^3LC states displaying identical spectral profiles and triplet energies (see Figure 2). Scheme 2 illustrates

Scheme 2^a



^aProposed Jablonski diagram showing photo-excitation to a singlet excited state (S_1), intersystem crossing (ISC) to a ligand-centered triplet excited state (^3LC), thermally accessible triplet metal-centered (^3MC) state, radiative decay (straight arrow), and nonradiative decay (wavy arrow) processes in complexes 1–4 at room temperature. Note that this diagram shows inexact energy levels, presenting the essence of our proposed mechanism.

the proposed schematic energy diagram. The ^3MC state has been reported to be involved in nonradiative decay and ligand dissociation mechanism in ruthenium (Ru) and Ir complexes because population to a ^3MC state, originating from the excitation of one electron from the occupied t_{2g} orbital to the unoccupied e_g orbital of the metal, often induces the elongation

or rupture of metal–N bonds.¹⁷ Assuming that the overall nonradiative rate constant k_{nr} is the sum of nonradiative rate constant for the ^3LC state (k_{nr}^{T}) and $k_{\text{nr}}^{\text{MC}}$ related to the population of ^3MC state as described by eq 3, one can expect that the fraction of $k_{\text{nr}}^{\text{MC}}$ governs the k_{nr} value, which in turn determines the excited-state lifetime τ of this cationic Ir complex system according to eq 2. The second term $k_{\text{nr}}^{\text{MC}}$ in eq 3 is given by eq 4,¹⁸ where we define k_a , k_b , and k_c as rate constants of activated surface crossing from the ^3LC state to the ^3MC state, repopulation of the ^3LC state, and nonradiative deactivation of the ^3MC state, respectively (also see Scheme 2).

$$k_{\text{nr}} = k_{\text{nr}}^{\text{T}} + k_{\text{nr}}^{\text{MC}} \quad (3)$$

$$k_{\text{nr}}^{\text{MC}} = k_a \frac{k_c}{k_b + k_c} \quad (4)$$

If ^3MC state decay to the ground state is much faster than the reverse reaction to the ^3LC state as reported in other Ir complexes ($k_b \ll k_c$),^{18c} then $k_{\text{nr}}^{\text{MC}}$ is approximated to be k_a . Conversely, if the ^3MC state decay is much slower than the reverse reaction to the ^3LC state ($k_b \gg k_c$), then eq 4 is simplified to $k_{\text{nr}}^{\text{MC}} = (k_a/k_b)k_c$, indicating that $k_{\text{nr}}^{\text{MC}}$ is strongly influenced by the k_a/k_b ratio because the two states are in equilibrium. In both limiting cases, $k_{\text{nr}}^{\text{MC}}$ is dependent on the relative energy position of the ^3MC state to the ^3LC state. The unstabilized ^3MC states of complexes 2 and 3 decrease either k_a or the k_a/k_b ratio, leading to lower $k_{\text{nr}}^{\text{MC}}$. In contrast, the stabilization of ^3MC state in complex 4 increases k_a or the k_a/k_b ratio and leads to higher $k_{\text{nr}}^{\text{MC}}$. Note, however, that the above interpretation is valid exclusively in the case when the introduced substituent groups change only the ^3MC level but do not affect the k_{nr}^{T} and k_{r} values remarkably. Whereas k_{r} values have proven to be quite similar, as seen in Table 1, we speculate that k_{nr}^{T} is also insensitive to the substitution because the phosphorescence spectral feature, triplet energy, and molecular framework of complexes 2 and 3 are analogous to those of complex 1.

The change of the ^3MC state energy level represented in Scheme 2 can be interpreted by the difference in ligand field splitting of the central Ir metal related to the bpy ancillary ligands. In complexes 2 and 3, a strong ligand field resulting from the increased degree of σ -donation ability shifts the ^3MC states to higher energy relative to their emissive ^3LC states. While further investigation is required using other bpy derivatives for better understanding, substitution of electron-donating groups at the para position to the coordinating nitrogen atom on the bpy could be effective for making the ligand field stronger.^{17g} For nonemissive complex 4, the electron-withdrawing group decreases the σ -donating ability of the bpy ligand, rendering the ^3MC state more stable than that of complex 1.

Phosphorescent Properties at Low Temperature. To better understand the excited state as well as the deactivation mechanism on the complexes 1–4, we measured their phosphorescence spectra and phosphorescence quantum yields in $\text{EtOH}-\text{CH}_3\text{OH}$ (1:1 v/v) at 77 K. The resulting spectra of complexes 1–3 are presented in Figure 4A. Their emission maxima and phosphorescence quantum yields are summarized in Table 2. As shown in Figure 4A, the phosphorescence spectra displayed vibronic progressions that became more resolved compared to those recorded at room temperature (Figure 2). The fact that these spectral features are nearly

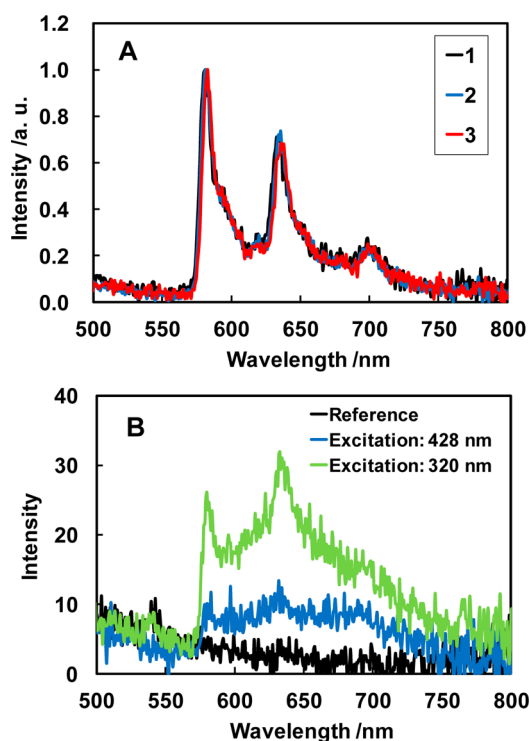


Figure 4. (A) Emission spectra of complexes 1–3 in EtOH–CH₃OH (1:1 v/v) at 77 K (excited at 430 nm). (B) Emission spectra of complex 4 in 2-MeTHF at 77 K (excited at 320 and 428 nm) and the reference without complex 4.

Table 2. Phosphorescent Properties of Complexes 1–4 in EtOH–CH₃OH (1:1 v/v) at 77 K

	λ_{em} (nm) ^a	E_{0-0} (eV) ^b	Φ^c
1	581, 634, 698	2.13	0.20
2	581, 635, 698	2.13	0.31
3	583, 636, 701	2.13	0.25
4 ^d	580, 634	2.14	0.09

^aPhosphorescence maxima. ^bTriplet energy. ^cPhosphorescence quantum yield. ^dMeasured in 2-MeTHF.

coincident with each other again indicates the similarity of complexes 1–3 in their emissive excited-state character and triplet energy ($E_{0-0} = 2.13$ eV). Complexes 1–3 showed a rigidochromic blue shift of 263 cm⁻¹ when changing the solvent from fluid CH₃CN (at room temperature) to low-temperature glasses (at 77 K). It is well-established that the magnitude of this rigidochromic blue shift is closely related to the degree of charge separation between the ground and excited states.¹⁹ Therefore, the observed small blue shift further suggests that

complexes 1–3 emit exclusively from btp-based triplet LC states rather than ³MLLCT or ³LLCT ones associated with the bpy ligand. Moreover, the btp-based ³LC state solely accounts for the observed invariable triplet energy (E_{0-0}) of the emissive excited states because the electronic nature of the btp moiety should not be influenced by the substituents on the bpy ligands. Yersin and co-workers previously studied excited state properties of Ir(btp)₂(acac) in detail,^{10b} and they assigned its emissive state to the ³LC state partially admixed with a MLCT character [Ir(d)→btp(π^*)]. We thus recorded the phosphorescence spectrum of Ir(btp)₂(acac) at 77 K for comparison and found a vibronic progression very similar to those of complexes 1–3, while the triplet state energy was lower by 0.08 eV (compare Supporting Information, Figure S5 with Figure 4A). Besides the similarity in spectral shape, the energy gaps between three vibronic peak maxima of Ir(btp)₂(acac) (1450 and 1407 cm⁻¹) are almost consistent with those of complexes 1–3 (1430–1464 and 1421–1458 cm⁻¹). Furthermore, the corresponding tris-cyclometalated complex *fac*-Ir(btp)₃ resembles complexes 1–3 and Ir(btp)₂(acac) in their phosphorescence spectral profile at 77 K.^{19a} These pieces of information provide additional evidence that the btp ligand, not the bpy ligand, is responsible for the phosphorescent LC states of complexes 1–3.

Complexes 1–3 became more emissive at 77 K as evidenced by their phosphorescence quantum yields in Table 2. It should be also emphasized that the phosphorescence quantum yield of complex 1 approached a value similar to those of complexes 2 and 3 although the quantum yield measured at room temperature was considerably lower than those of complexes 2 and 3 (compare Table 2 with Table 1). It therefore seems reasonable to explain that the ³MC states of complexes 1–3 are located above the ³LC states, and cooling the sample solution to 77 K leads to lower population in the ³MC state. Under such conditions, the contribution of k_{nr}^{MC} in eq 3 can be neglected since the k_a value should be much lower than that at room temperature, that is, $k_a \ll k_b$ or $k_a \ll k_{nr}^T$. On the other hand, complex 4 did not luminesce clearly in the range of 500–900 nm even at 77 K as depicted in Supporting Information, Figure S6, and thus the very weak emission did not allow us to conclude whether or not it comes from complex 4. However, more intense phosphorescence was observed when 2-methyltetrahydrofuran (2-MeTHF) was used as a glass-forming solvent instead of EtOH–CH₃OH (see Figure 4B).²⁰ In addition, the intensity was enhanced when the excitation wavelength was changed from 428 nm to shorter wavelength where complex 4 can absorb larger amounts of photons, confirming that the observed emission originates from complex 4. It is also important to note that the triplet energy of the emissive state is identical to those of complexes 1–3. The

Table 3. Electrochemical Data of Complexes 1–4

	$E_{1/2}^{red}$ (ΔE) ^a (V)	$E_{1/2}^{ox}$ (ΔE) ^a (V)	$E_{1/2}^{ox} - E_{1/2}^{red}$ (V)	E^{red*} (V) ^b	E^{ox*} (V) ^c
1	-1.15 (0.07)	1.25 (0.08), 1.57 (0.12)	2.40	0.98	-0.88
2	-1.23 (0.07)	1.24 (0.09), 1.58 (0.12)	2.47	0.90	-0.89
3	-1.25 (0.08)	1.21 (0.10), 1.56 (0.12)	2.46	0.88	-0.92
4	-0.75 ^d , -1.45 ^d	1.31 (0.09), 1.59 (0.12)	2.06	1.39	-0.83

^aDetermined by CV in deaerated CH₃CN containing 0.1 M *n*-Bu₄NClO₄, and reported vs Ag/AgCl (ferrocene/ferrocenium: $E_{1/2} = 0.56$ V vs Ag/AgCl). Peak-to-peak separation (ΔE) is given in parentheses at a scan rate of 100 mV/s⁻¹. ^bExcited-state reduction potential (vs Ag/AgCl) estimated using $E^{red*} = E_{1/2}^{red} + E_{0-0}$, where E_{0-0} denotes triplet energy estimated from the phosphorescence data at 77 K. ^cExcited-state oxidation potential (vs Ag/AgCl) estimated using $E^{ox*} = E_{1/2}^{ox} - E_{0-0}$. ^dIrreversible.

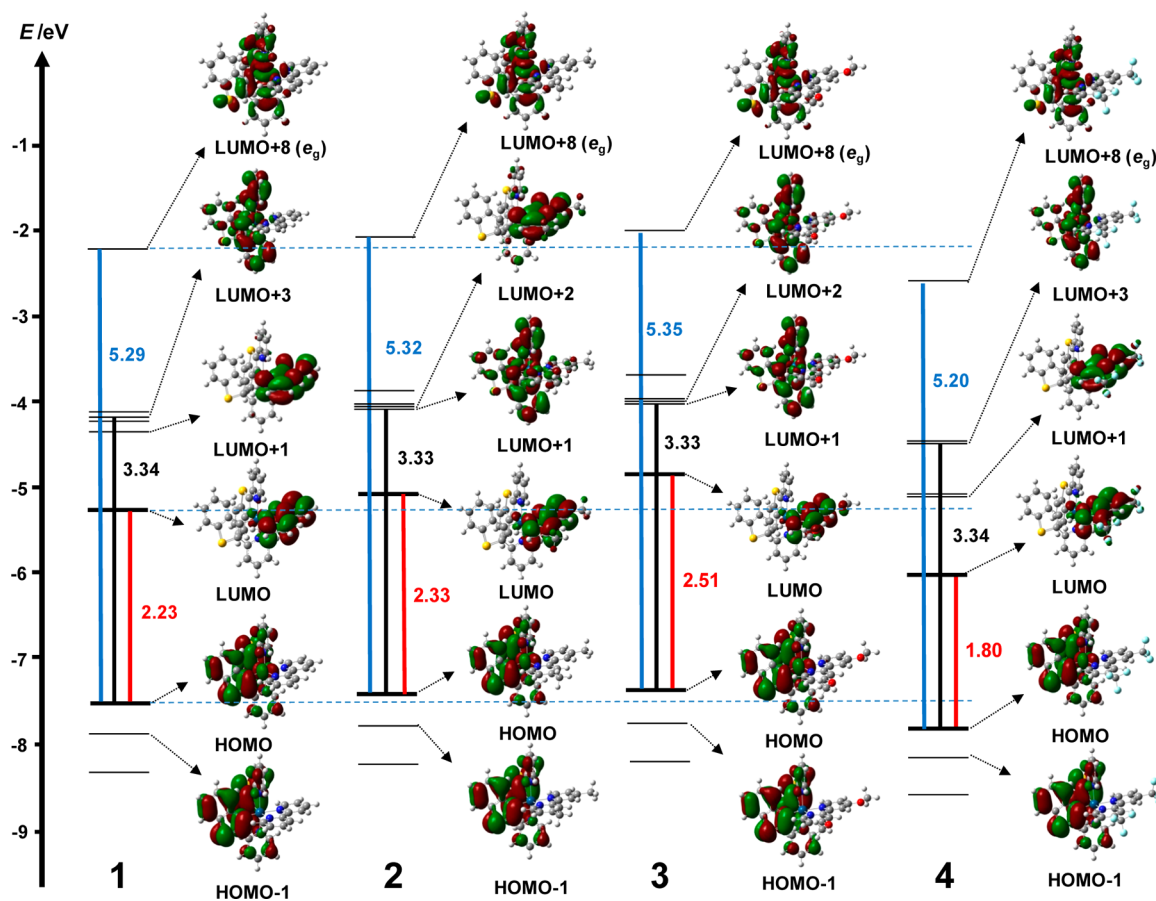


Figure 5. Schematic diagram showing the MO distributions and their energy levels of complexes 1–4 from DFT calculations (B3LYP, 6-31G basis set on C, H, N, O, F, S atoms; LANL2DZ basis set on the Ir atom). Black, red, and blue vertical lines schematically indicate the energy gaps corresponding to LC, MLLCT, and d–d transitions, respectively.

phosphorescence quantum yield was determined to be less than half of the values of complexes 1–3. This implies that the ^3MC state level of complex 4 is close in energy to the ^3LC state, and the k_a value remains high so that the nonradiative deactivation proceeds through the ^3MC state even at 77 K. Taken together, these low-temperature experiments leave little doubt that the thermally accessible ^3MC state is pertinent to understand the photophysical behavior of the complexes.

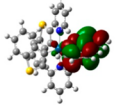
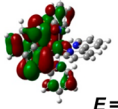
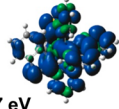

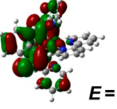
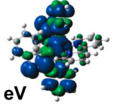
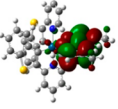
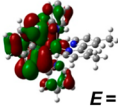
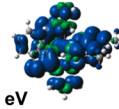

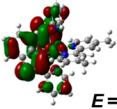
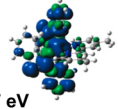
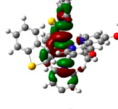
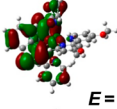
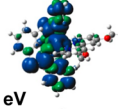
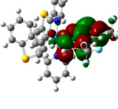
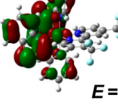
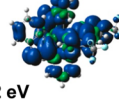
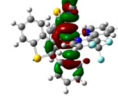
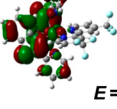
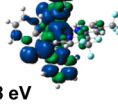
Electrochemical Properties. Electrochemical measurements are one of the useful experimental techniques to estimate the energy levels of the highest occupied molecular orbital (HOMO) and lowest unoccupied molecular orbital (LUMO) of the ground state of Ir complexes. We therefore carried out cyclic voltammetry (CV) in CH_3CN to investigate the redox behavior of complexes 1–4. The electrochemical data obtained were collected in Table 3. Cyclic voltammograms are available in the Supporting Information (Figures S7 and S8). All the complexes displayed two reversible oxidation waves and a single reversible reduction wave, with some exceptions. The first oxidation couple between 1.21 and 1.31 V (vs Ag/AgCl) is assigned to Ir-based oxidation ($\text{Ir}^{\text{III}}/\text{Ir}^{\text{IV}}$), and the subsequent oxidation between 1.56 and 1.59 V most likely occurs at the benzo[*b*]thiophene moiety of the btp ligand. This assignment is supported by the observation that the first oxidation potential is influenced by the substituents introduced on the bpy ligand, whereas the second oxidation appears to be independent of these substituents. Furthermore, we have confirmed that btp shows an irreversible oxidation at 1.83 V, which is more positive

than the corresponding btp-based oxidation in complexes 1–4. We suppose that this difference depends on whether or not the carbon at the 3-position of benzo[*b*]thiophene is coordinated with Ir metal. The reduction process takes place on the bpy ligand for all of the complexes.

It is evident from Table 3 that the electrochemical properties correlate well with the nature of the substituent groups on the ancillary ligand. The electron-donating groups cathodically shifted both the oxidation and reduction potentials, while the electron-withdrawing CF_3 group induced appreciable anodic shift in the redox potentials. In other words, the electron-donating group destabilizes the HOMO and LUMO of the parent complex; meanwhile, the electron-withdrawing group stabilizes these frontier orbitals. However, it should be highlighted that the substituent effect was found to be more dominant in reduction potential than in oxidation potential, probably due to localization of the LUMO on the bpy ligand, thereby resulting in distinct HOMO–LUMO energy gaps of complexes 1–4.

Computational Study. Since P. J. Hay reported theoretical studies on cyclometalated Ir complexes,²¹ density functional theory (DFT) has been accepted as a powerful technique to understand the ground and excited electronic states of cyclometalated Ir complexes as well as the deactivation process via thermally accessible ^3MC (dd) states.^{1e,18c,22} Preliminary DFT calculations were thus performed for complexes 1–4 at the B3LYP level using the 6-31G basis set on C, H, N, O, F, S atoms, and the LANL2DZ basis set was used on the Ir atom to

Table 4. The Highest Singly Occupied Molecular Orbital (HSOMO), the Lowest Singly Occupied Molecular Orbital (LSOMO), and Spin Density Distributions for the Calculated Triplet States of Complexes 1–4

1–4	T_1			3MC		
	HSOMO	LSOMO	Spin density	HSOMO	LSOMO	Spin density
1			 $E = 1.87 \text{ eV}$			 $E = 2.55 \text{ eV}$
2			 $E = 1.95 \text{ eV}$			 $E = 2.57 \text{ eV}$
3 ^a	—	—	—			 $E = 2.59 \text{ eV}$
4			 $E = 1.42 \text{ eV}$			 $E = 2.48 \text{ eV}$

^aThe optimized structure of the T_1 state was unsymmetric.

understand the properties of our new cationic Ir complexes. First, we carried out geometry optimization on the ground state of each complex. All the calculations successfully converged to provide the optimized geometries with molecular orbital (MO) structures and the energy levels displayed in Figure 5. The DFT calculation of complex 1 revealed that the HOMO is composed of $\text{btp-}\pi$ and Ir-d orbitals, whereas the LUMO is largely localized on the bpy ligand with little Ir-metal orbital character. As a consequence, introducing the substituent groups on the bpy ligand affects the LUMO but has minor effects on the HOMO. The calculations of complexes 2–4 demonstrated that the electron-donating Me and OMe groups destabilize the LUMO, and the electron-withdrawing CF_3 group leads to the LUMO stabilization. This trend in substituent effect and the HOMO–LUMO energy gap is to some extent in agreement with the electrochemical data of complexes 1–4 (see Table 3). In contrast, the energy gap that corresponds to LC transition (benzo[*b*]thiophene→pyridine moiety of the btp) was found to be independent of the substituents owing to the absence of MO distributions on the bpy ligand. It is also noteworthy that the energy gap corresponding to the d–d ($\text{HOMO}\rightarrow e_g$) transition appears to be susceptible to the substituents even though the HOMO and LUMO+8 (e_g) are not expanded to the bpy ligand. It is likely that the energy level of LUMO+8 (e_g) reflects the change in ligand field splitting of the Ir metal, which is induced by the indirect substituent effect.

To theoretically explore the excited-state properties of complexes 1–4, the lowest triplet state (T_1) and the 3MC state were optimized at the unrestricted B3LYP level as the lowest state with the triplet multiplicity. To locate the 3MC state, we adopted a strategy reported by P. Persson and co-workers.^{17c} The starting structures were constructed to lower the energy of the unoccupied e_g orbitals by displacing the pyridyl moieties of the btp ligands away from the iridium core. Table 4 depicts the resulting optimized structures, their MOs, spin density distributions, and the calculated triplet energy values for the T_1 and 3MC states. The structures placed in the

right column were assigned as 3MC states on the basis of the following points: (1) The LSOMO and HSOMO distributions showed a resemblance to the topology of $\text{HOMO}\rightarrow\text{LUMO}+8$ (e_g) excitation in Figure 5. (2) A large amount of spin density was centered at the Ir metal. (3) The axial Ir–N bonds were much longer than those of the optimized ground state structures, as also suggested in other recent works dealing with 3MC states of Ir complexes.^{1e,22f,g}

Importantly, the electron-donating groups were found to increase the triplet energy of the 3MC state (Table 4). On the other hand, the CF_3 group decreased the 3MC triplet energy. Although the degree of variation was somewhat smaller than our expectation, this tendency provides additional support for our proposed mechanism behind the changeable excited-state lifetime of the btp-based Ir complex. The lowest triplet state (T_1) is generally responsible for the observed phosphorescence. However, there is poor agreement between the experimental and computational results: the DFT calculations generated the T_1 states corresponding to the MLLCT ($\text{HOMO}\rightarrow\text{LUMO}$) transition, of which triplet energy varied depending on the substituents due to major contribution of the bpy moiety on the HSOMO, although our experimental data strongly suggested that the emissive states of complexes 1–4 are ascribed to the btp LC state. The experimentally determined triplet energies (2.13–2.14 eV) are nearly constant for complexes 1–4 and higher than the calculated T_1 energies (1.87 eV for 1; 1.95 eV for 2; 1.42 eV for 4). At present, we have no definitive explanation for this contradiction, but we assume that the actual emissive state might be a higher-lying triplet state, such as T_2 and T_3 states, consisting of LC state. Several research groups independently reported that Kasha's rule²³ is not valid for rare examples showing dual emission from different excited states in Ru and Ir complexes.²⁴ In our case, it can be presumed that internal conversion from the T_2 (or T_3) to T_1 state is slow enough to give way to the radiative decay process from the T_2 (or T_3) state, and that there is a large energy gap or large energy barrier between these two triplet

states with different MO distributions. To estimate possible triplet excited states of complexes 1–4, time-dependent DFT (TD-DFT) calculations were performed. As summarized in Supporting Information, Table S1, these calculations predicted that triplet energies of T_3 (complex 1), T_2 (complex 2), T_2 (complex 3), and T_6 (complex 4) states are 2.13 eV, 2.15 eV, 2.16 eV, and 2.12 eV, respectively. All these triplet states can be described as btp-based LC states. Importantly, the experimentally determined 3LC state energies (2.13–2.14 eV) are in better agreement with these higher-lying triplet energies than the computed T_1 state energies that are much lower compared to the T_2 energies. In addition, the substituents remarkably change the T_1 energy. This finding is consistent with the trend of the results from the geometry optimization at the unrestricted B3LYP level (Table 4). Interestingly, complex 4 was predicted to have several triplet states, located between the T_1 (MLLCT_{bpy}) and T_6 (LC_{btp}) states, some of which are degenerate states assigned to LLCT. As seen in Figure 4B, complex 4 appeared to exhibit broad phosphorescence along with a vibronic progression similar to those of complexes 1–3 at 77 K. This broad spectral characteristic might reflect the admixture of the T_2 – T_5 states. On the basis of the results above and exclusion of the following two scenarios, we tentatively concluded that the lowest-lying T_1 states corresponding to the HOMO→LUMO excitation do exist in complexes 1–4, but do not participate in their deactivation processes.

First, if the T_1 states were “accessible non-emissive, short-lived states”, all the complexes would be nonemissive at room temperature and 77 K, as the combined DFT and TD-DFT calculations indicated that the T_1 states are much lower in energy than the T_2 and 3MC ones. Moreover, this type of T_1 state associated with the bpy ligand is generally emissive (also see the following paragraph), and there is neither strong evidence nor literature suggesting that it could be a nonemissive and short-lived state.

Second, if the T_1 states were “accessible emissive states”, complexes 1–4 would exhibit phosphorescence with remarkably different emission maxima at room temperature and 77 K. This case can be found in well-known $[\text{Ir}(\text{ppy})_2(\text{bpy})]^+$ compounds, of which emissive excited states were assigned to the lowest-lying Ir-to-bpy 3MLCT state.^{19b} It has actually been reported that introduction of electron-donating *t*-butyl groups on the bpy ligand increases the emission energy by 391 cm^{-1} ($583\text{ nm} \rightarrow 570\text{ nm}$).²⁵ However, this trend does not match our case with the btp-based Ir complexes. Because such different photophysics between the $[\text{Ir}(\text{btp})_2(\text{bpy})]^+$ complexes and the $[\text{Ir}(\text{ppy})_2(\text{bpy})]^+$ complexes is somewhat surprising, it is certain that our btp-based Ir complexes will offer a new interesting topic for research in the field of phosphorescent iridium complexes. Further investigation is currently underway to corroborate our proposed scheme of the photophysics of complexes 1–4.

Photoinduced Electron-Transfer Reactions Using Complexes 1–4 as Sensitizers. Finally, we investigated whether the long-lived excited states of complexes 2 and 3 are reflected in their photosensitizing properties in photoinduced electron-transfer (PET) reaction. For this purpose, we employed a quite simple three-component system composed of triethanolamine (TEOA) as a sacrificial electron donor, Ir complex as a sensitizer, and methylviologen chloride (MVCl_2) as an electron acceptor. This PET reaction was selected because the reduced form of MV^{2+} (MV radical cation, $\text{MV}^{\bullet+}$) is known to exhibit a characteristic absorption centered at 604 nm,

allowing for a detailed kinetic study by monitoring $\text{MV}^{\bullet+}$ concentration during the course of irradiation.²⁶ Furthermore, MV^{2+} is able to serve as an electron mediator in a number of photochemical hydrogen generating systems,²⁷ and therefore, the use of MV^{2+} in this Study may find additional applications in our future work.

Solutions containing TEOA (302 mM), Ir complex 1–4 (20.0 μM), and MVCl_2 (130 μM) in $\text{CH}_3\text{CN}-\text{H}_2\text{O}$ (1:1 v/v) were bubbled with argon gas for 20 min and then irradiated using a xenon arc lamp through optical glass filters ($454 \pm 52\text{ nm}$). As seen in Figure 6 and Supporting Information, Figures

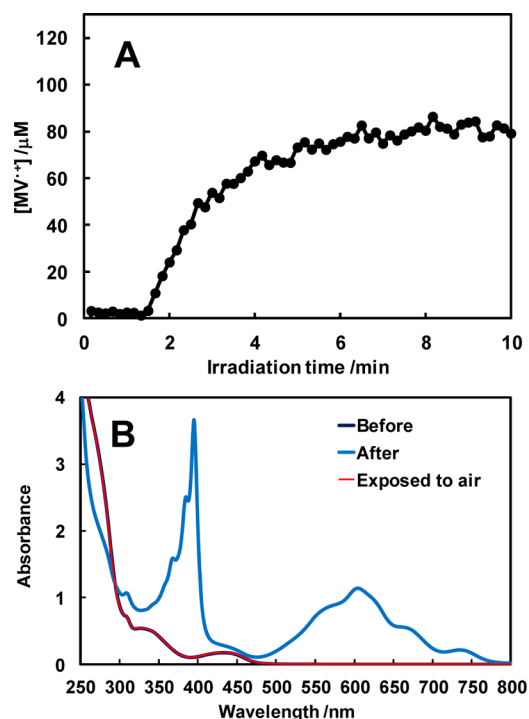


Figure 6. (A) Change in the concentration of $\text{MV}^{\bullet+}$ vs irradiation time for the PET reaction with Ir sensitizer 2. (B) Absorption spectra before and after the PET reaction with Ir sensitizer 2, along with the spectrum of the solution exposed to air after the reaction.

S9 and S10, irradiation of the solutions containing complexes 1–3 resulted in accumulation of $\text{MV}^{\bullet+}$, which is an indicator of the PET reaction progress. Our control experiment verified that the Ir sensitizer is required for the observation of $\text{MV}^{\bullet+}$. Figure 6B and Supporting Information, Figures S9B and S10B show the absorption spectra of the solution containing TEOA, complex 1–3, and MV^{2+} before and after the reaction. The absorption spectra of the sample solutions exposed to air just after the reaction perfectly matched their spectra before the reaction, demonstrating that complexes 1–3 are stable enough to drive this PET reaction. However, an induction period of 10–30 min was always observed in the reaction with complex 1, despite repeating the experiment several times under the same conditions. For all the PET reactions using complexes 1–3, the initial rates of $\text{MV}^{\bullet+}$ formation v_i were obtained as derivatives at the initial part of each $\text{MV}^{\bullet+}$ accumulation curve. These initial rates are summarized in Table 5.

As we expected, the PET reaction using complex 2 or 3 was dramatically faster than that with complex 1, as clearly shown on their initial rates of $\text{MV}^{\bullet+}$ formation ($1.79\ \mu\text{M min}^{-1}$ for complex 1, $50.8\ \mu\text{M min}^{-1}$ for complex 2, $43.9\ \mu\text{M min}^{-1}$ for

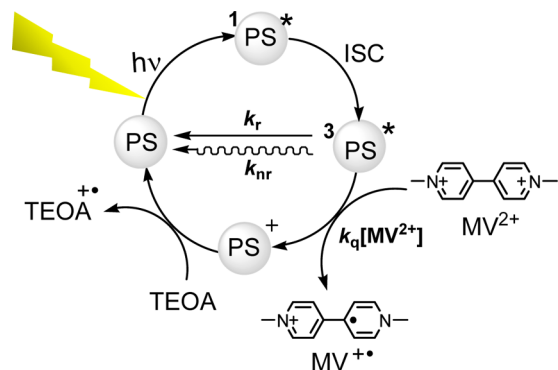
Table 5. Results of the PET Reactions Using Complexes 1–4^a and Kinetic Parameters of Quenching by MV²⁺ and TEOA in CH₃CN–H₂O (1:1 v/v)

sensitizer	v_i ($\mu\text{M min}^{-1}$) ^b	TEOA		MV ²⁺		
		K_{SV} (M^{-1}) ^c	k_q ($\text{M}^{-1} \text{s}^{-1}$) ^d	K_{SV} (10^3M^{-1}) ^c	k_q ($10^8 \text{M}^{-1} \text{s}^{-1}$) ^d	k_q [MV^{2+}] (10^5s^{-1}) ^e
1	1.79	no quenching		0.269	12.2	1.59
2	50.8	no quenching		2.24	8.18	1.06
3	43.9	no quenching		2.70	8.31	1.08
4	<0.1					

^aReaction condition: TEOA (302 mM)/Ir complex (20.0 μM)/MVCl₂ (130 μM) in CH₃CN–H₂O (1:1 v/v), λ : 454 \pm 52 nm ^bInitial rate of MV^{•+} generation. ^cStern–Volmer quenching constant. ^dQuenching rate constant calculated using $k_q = K_{\text{SV}}/\tau_0$, where τ_0 stands for phosphorescence lifetime of the complex measured in deaerated CH₃CN–H₂O (1:1 v/v) without the quencher (1: 220 ns, 2: 2.74 μs , 3: 3.25 μs). ^eRate constant for the quenching process ($[\text{MV}^{2+}] = 130 \mu\text{M}$).

complex 3). In contrast to the complexes having electron-donating groups, complex 4 did not generate MV^{•+} even after 60 min of continuous irradiation.

To obtain further information about the photosensitizing properties of the Ir complexes and the reaction mechanism, we performed Stern–Volmer quenching experiments on the complexes, using TEOA and MVCl₂ in CH₃CN–H₂O (1:1 v/v). The resulting kinetic parameters from the quenching experiments are listed in Table 5. In addition, photophysical data of complexes 1–3 in CH₃CN–H₂O (1:1 v/v) are separately collected in Supporting Information, Table S4. Whereas TEOA did not quench the emissions of complexes 1–3 at all, quenching occurred when MVCl₂ was used, with Stern–Volmer quenching constants K_{SV} of 269 M⁻¹, 2240 M⁻¹, and 2700 M⁻¹. Hence, we propose that the PET reaction proceeds via an oxidative quenching pathway, as illustrated in Scheme 3. First, an Ir(III) complex absorbs visible light to

Scheme 3. Proposed Reaction Mechanism Involving an Oxidative Quenching Pathway of the Ir Photosensitizer (PS) Competitive with Intramolecular Decay Processes

become the triplet excited state. Second, the photoexcited Ir(III) complex undergoes oxidative quenching by MV²⁺ to produce MV^{•+}. In parallel, the resultant Ir(IV) species is reduced by TEOA to regenerate the Ir(III) complex.

As anticipated, the K_{SV} values of complexes 2 and 3 are much higher than that of complex 1 despite their similar quenching rate constants (k_q). Rate constants for the bimolecular reaction between the excited Ir complex (³PS*) and MV²⁺ were then determined to be (1.06–1.59) $\times 10^5 \text{s}^{-1}$ under the same condition as the PET reactions, that is, $[\text{MV}^{2+}] = 130 \mu\text{M}$. These bimolecular rate constants, as well as nonradiative rate constants of complexes 1–3 in Supporting Information, Table S4, suggest that the quenching of complexes 2 and 3 by MV²⁺ can compete with the intramolecular decay processes, while the

nonradiative decay of complex 1 is too fast to precede the PET reaction. More specifically, the nonradiative rate constant of complex 3 ($k_{\text{nr}} = 2.9 \times 10^5 \text{s}^{-1}$) is only 2.7 times higher than the bimolecular rate constant ($k_q[\text{MV}^{2+}] = 1.08 \times 10^5 \text{s}^{-1}$). On the other hand, the nonradiative rate constant of complex 1 ($k_{\text{nr}} = 5 \times 10^6 \text{s}^{-1}$) is approximately 30 times higher than the bimolecular rate constant ($k_q[\text{MV}^{2+}] = 1.59 \times 10^5 \text{s}^{-1}$). Note that one does not need to take account of the radiative decay pathway because complexes 1–3 possess radiative decay rate constants that are 1–2 orders of magnitude smaller than the nonradiative rate constants (see Supporting Information, Table S4). Complex 4 did not act as an effective sensitizer as well as complex 1, most probably due to having an even faster nonradiative decay of the triplet excited-state than complex 1 has, although the nonemissive property of complex 4 precluded estimation of its kinetic parameters. We should also consider that the excited states of complexes 1, 2, 3, and 4 ($E^{\text{ox}*} = -0.88 \text{V}$; -0.89V ; -0.92V ; -0.83V) are thermodynamically capable of reducing MV²⁺ ($E^{\text{red}} = -0.42 \text{V vs Ag/AgCl}^{28}$), and the $E_{1/2}^{\text{ox}}$ values of these complexes (1.25 V; 1.24 V; 1.21 V; 1.31 V) are high enough so that PS⁺ oxidizes TEOA ($E^{\text{ox}} = 0.61 \text{V vs Ag/AgCl}^{29}$). In other words, complexes 1–4 have almost identical positive driving forces for each quenching and regeneration process in this PET reaction. Gathering the above experimental information, we can conclude that the differences in the excited-state lifetime kinetically control this PET reaction; that is, the electron-donating groups are effective not only for producing the long-lived excited state of the btp-based Ir complex, but also for improving its photosensitizing properties.

CONCLUSIONS

A series of cationic Ir complexes comprising two btp ligands and one bpy ancillary ligand with different substituents have been synthesized and examined for their photophysical, electrochemical, and photosensitizing properties. We have unexpectedly found that introducing electron-donating groups on the bpy ligand render the ³LC state long-lived without changing the absorption and emission spectral features. This is reasonably explained by assuming that the increased σ -donating character preferentially destabilizes a short-lived, nonemissive ³MC state. On the other hand, the ³MC state may be populated easily in the complex substituted with the electron-withdrawing CF₃ groups, making the complex nonemissive at room temperature. Furthermore, the long excited-state lifetime, as a result of the introduction of electron-donating groups, contributes to improved photosensitizing properties of the btp-based Ir complex in photoinduced electron-transfer reaction between TEOA and MV²⁺.

A pioneering work by Thompson's group showed that manipulation of the ^3MC state can be accomplished by the use of *N*-heterocyclic carbene ligands having strong ligand field in tris-cyclometalated Ir complexes,^{17d,30} but this strategy seems to be limited just to development of blue to near-UV phosphorescent Ir materials. Also, recent studies related to the ^3MC state tuning have focused only on phosphorescence quantum efficiency improvement toward $\text{LEC}^{1\text{e},18\text{c},22\text{g}}$ and deep-blue phosphorescent OLED applications.^{30,31} Our Study has first uncovered a proof of concept demonstrating that simple substitution on the diimine ancillary ligand can control the ^3MC state of the bis-cyclometalated cationic Ir complex to finely tune its excited-state and photosensitizing properties. This new concept might bring an important and useful perspective in further developing new sensitizers based on bis-cyclometalated cationic Ir complexes.

EXPERIMENTAL SECTION

General Information. ^1H NMR spectra were recorded on a Bruker Avance III 500 MHz spectrometer, and chemical shifts were referenced to tetramethylsilane ($\text{Si}(\text{CH}_3)_4$). Fast atom bombardment (FAB) mass spectra were recorded using a JEOL JMS-600H mass spectrometer. Elemental analyses were performed using a YANACO CHN corder MT-6 at the Microanalytical Laboratory (Department of Chemistry, School of Science, The University of Tokyo). UV-vis absorption spectra were recorded on a JASCO V-560 spectrometer. Photoluminescence excitation spectra were recorded on a Hitachi High-Technologies FL7000.

Chemicals. Iridium(III) chloride trihydrate, 2,2'-bipyridyl (bpy), and ethylene glycol were purchased from Kanto Chemical Co., Inc. Ammonium hexafluorophosphate (NH_4PF_6), 4,4'-dimethyl-2,2'-bipyridyl, triethanolamine (TEOA), and methylviologen chloride trihydrate ($\text{MVC}_2\cdot 3\text{H}_2\text{O}$) were purchased from Sigma-Aldrich. 2-(2-Pyridyl)-benzo[*b*]thiophene (btp) and 4,4'-dimethoxy-2,2'-bipyridyl were purchased from Tokyo Chemical Industry (TCI) Co., Ltd. These chemicals were used without any previous purification. $\text{Ir}(\text{btp})_2(\text{acac})^{10\text{a}}$ and 4,4'-bis(trifluoromethyl)-2,2'-bipyridyl³² were synthesized according to previously reported procedures. Acetonitrile (Dotite Spectrosol) for spectroscopic measurements were purchased from Wako Pure Chemical Industries, Ltd.

Synthesis of Iridium(III) Bis[2-(benzo[*b*]thiophen-2-yl)-pyridinato-*N,C^3'*](2,2'-bipyridine) Hexafluorophosphate (1). A mixture of iridium(III) chloride trihydrate (0.150 g, 0.425 mmol) and 2-(2-pyridyl)benzo[*b*]thiophene (0.188 g, 0.900 mmol) in 2-ethoxyethanol/water (12 mL; 3:1 v/v) was heated at 115 °C for 24 h under nitrogen. After cooling the reaction mixture to room temperature, the precipitate was filtered off and washed with ethanol. The resulting orange solid was dried under vacuum to yield 84% of Ir(III) μ -chloro-bridged dimer complex **5** (0.232 g, 0.179 mmol).

A mixture of dimer complex **5** (0.077 g, 0.059 mmol) and 2,2'-bipyridyl (bpy: 0.019 g, 0.12 mmol) in ethylene glycol (5.0 mL) was heated at 150 °C for 24 h under nitrogen. The reaction mixture was poured into water (40 mL) and washed with diethyl ether (40 mL \times 2). To the aqueous layer was added ammonium hexafluorophosphate (0.533 g, 3.27 mmol), and the resulting orange solid was filtered off, washed with water, and air-dried for 19 h. The solid was dissolved in acetone (ca. 70 mL), and the volume of the solution was reduced to ca. 15 mL by rotary evaporation under vacuum. To the solution was added *n*-hexane, and the produced precipitate was filtered off and washed with *n*-hexane. The obtained solid was dried under reduced pressure to yield complex **1** as an orange solid (0.075 g, 0.082 mmol, 70% yield). ^1H NMR (500 MHz, $\text{DMSO}-d_6$) δ 8.93 (d, *J* = 8.0, 2H), 8.31 (t, *J* = 8.0 Hz, 2H), 8.01 (t, *J* = 8.0 Hz, 2H), 7.94 (d, *J* = 8.0 Hz, 2H), 7.93 (d, *J* = 8.0 Hz, 2H), 7.85 (d, *J* = 6.0 Hz, 2H), 7.70 (t, *J* = 7.0 Hz, 2H), 7.68 (d, *J* = 6.0 Hz, 2H), 7.22 (t, *J* = 8.0 Hz, 2H), 7.10 (t, *J* = 7.0 Hz, 2H), 6.89 (t, *J* = 8.0 Hz, 2H), 5.95 (d, *J* = 8.0 Hz, 2H). Anal. Calcd for $\text{C}_{36}\text{H}_{24}\text{F}_6\text{IrN}_4\text{PS}_2\cdot\text{H}_2\text{O}\cdot 0.2\text{CH}_3\text{COCH}_3$: C, 46.59; H, 2.91;

N, 5.94. Found: C, 46.86; H, 3.18; N, 5.74%. FAB mass spectrometry (MS) (*m/e*): found, 613 $[\text{M}-\text{bpy}-\text{PF}_6^-]^+$; 769 $[\text{M}-\text{PF}_6^-]^+$.

Synthesis of Iridium(III) Bis[2-(benzo[*b*]thiophen-2-yl)-pyridinato-*N,C^3'*](4,4'-dimethyl-2,2'-bipyridine) Hexafluorophosphate (2). A mixture of dimer complex **5** (0.060 g, 0.046 mmol) and 4,4'-dimethyl-2,2'-bipyridyl (bpyMe: 0.017 g, 0.092 mmol) in ethylene glycol (3.9 mL) was heated at 150 °C for 18 h under nitrogen. The reaction mixture was poured into water (40 mL) and washed with diethyl ether (40 mL \times 2). To the aqueous layer was added ammonium hexafluorophosphate (0.412 g, 2.53 mmol), and the resulting solid was extracted with dichloromethane (40 mL \times 2). The combined organic layers were washed with water and dried over Na_2SO_4 . The obtained solution was filtered to remove the drying reagent, and the solvent was removed by rotary evaporation under vacuum. The resulting crude product was purified by column chromatography on silica gel (solvent: methanol/dichloromethane, 1:4 v/v), followed by recrystallization from ethanol through dichloromethane vapor diffusion to yield complex **2** as orange-red crystals (0.066 g, 0.070 mmol, 76% yield). ^1H NMR (500 MHz, $\text{DMSO}-d_6$) δ 8.79 (s, 2H), 8.00 (t, *J* = 8.0 Hz, 2H), 7.93 (d, *J* = 8.0 Hz, 2H), 7.92 (d, *J* = 8.0 Hz, 2H), 7.68 (d, *J* = 6.0 Hz, 2H), 7.65 (d, *J* = 6.0 Hz, 2H), 7.52 (d, *J* = 6.0 Hz, 2H), 7.22 (t, *J* = 8.0 Hz, 2H), 7.11 (t, *J* = 7.0 Hz, 2H), 6.88 (t, *J* = 8.0 Hz, 2H), 5.95 (d, *J* = 8.0 Hz, 2H), 2.54 (s, 6H). Anal. Calcd for $\text{C}_{38}\text{H}_{28}\text{F}_6\text{IrN}_4\text{PS}_2\cdot\text{H}_2\text{O}$: C, 47.54; H, 3.15; N, 5.84. Found: C, 47.57; H, 3.18; N, 5.68%. FAB MS (*m/e*): found, 613 $[\text{M}-\text{bpyMe}-\text{PF}_6^-]^+$; 797 $[\text{M}-\text{PF}_6^-]^+$.

Synthesis of Iridium(III) Bis[2-(benzo[*b*]thiophen-2-yl)-pyridinato-*N,C^3'*](4,4'-dimethoxy-2,2'-bipyridine) Hexafluorophosphate (3). A mixture of dimer complex **5** (0.060 g, 0.046 mmol) and 4,4'-dimethoxy-2,2'-bipyridyl (bpyOMe: 0.020 g, 0.092 mmol) in ethylene glycol (3.9 mL) was heated at 150 °C for 21 h under nitrogen. The reaction mixture was poured into water (40 mL) and washed with diethyl ether (40 mL \times 2). To the aqueous layer was added ammonium hexafluorophosphate (0.412 g, 2.53 mmol), and the resulting solid was extracted with dichloromethane (40 mL \times 2). The combined organic layers were washed with water and dried over Na_2SO_4 . The solution was filtered to remove the drying reagent, and the solvent was removed by rotary evaporation under vacuum. The obtained crude product was purified by column chromatography on silica gel (solvent: methanol/dichloromethane, 1:4 v/v), followed by recrystallization from ethanol through dichloromethane vapor diffusion to yield complex **3** as orange crystals (0.057 g, 0.058 mmol, 64% yield). ^1H NMR (500 MHz, $\text{DMSO}-d_6$) δ 8.50 (s, 2H), 8.01 (t, *J* = 8.0 Hz, 2H), 7.93 (d, *J* = 8.0 Hz, 2H), 7.92 (d, *J* = 8.0 Hz, 2H), 7.73 (d, *J* = 6.0 Hz, 2H), 7.57 (d, *J* = 6.0 Hz, 2H), 7.30 (d, *J* = 6.0 Hz, 2H), 7.21 (t, *J* = 8.0 Hz, 2H), 7.13 (t, *J* = 7.0 Hz, 2H), 6.89 (t, *J* = 8.0 Hz, 2H), 5.96 (d, *J* = 8.0 Hz, 2H), 3.99 (s, 6H). Anal. Calcd for $\text{C}_{38}\text{H}_{28}\text{F}_6\text{IrN}_4\text{O}_2\text{PS}_2\cdot 0.5\text{CH}_2\text{Cl}_2$: C, 45.49; H, 2.88; N, 5.51. Found: C, 45.27; H, 3.02; N, 5.33%. FAB MS (*m/e*): found, 613 $[\text{M}-\text{bpyOMe}-\text{PF}_6^-]^+$; 829 $[\text{M}-\text{PF}_6^-]^+$.

Synthesis of Iridium(III) Bis[2-(benzo[*b*]thiophen-2-yl)-pyridinato-*N,C^3'*](4,4'-bis(trifluoromethyl)-2,2'-bipyridine) Hexafluorophosphate (4). A mixture of dimer complex **5** (0.088 g, 0.068 mmol) and 4,4'-bis(trifluoromethyl)-2,2'-bipyridyl (bpyCF₃: 0.040 g, 0.14 mmol) in ethylene glycol (5.9 mL) was heated at 150 °C for 45 h under nitrogen. The reaction mixture was poured into water (40 mL) and washed with diethyl ether (40 mL \times 2). To the aqueous layer was added ammonium hexafluorophosphate (0.610 g, 3.74 mmol), and the resulting solid was extracted with dichloromethane (40 mL \times 2). The combined organic layers were washed with water and dried over Na_2SO_4 . The solution was filtered to remove the drying reagent, and the solvent was removed by rotary evaporation under vacuum. The obtained crude product was purified by column chromatography on silica gel (solvent: methanol/dichloromethane, 1:6 v/v), followed by recrystallization from ethanol through dichloromethane vapor diffusion to yield complex **4** as dark-brown crystals (0.078 g, 0.074 mmol, 55% yield). ^1H NMR (500 MHz, $\text{DMSO}-d_6$) δ 9.64 (s, 2H), 8.13 (d, *J* = 6.0 Hz, 2H), 8.09 (d, *J* = 6.0 Hz, 2H), 8.04 (t, *J* = 8.0 Hz, 2H), 7.95 (d, *J* = 8.0 Hz, 2H), 7.94 (d, *J* = 8.0 Hz, 2H), 7.82 (d, *J* = 6.0 Hz, 2H), 7.24 (t, *J* = 8.0 Hz, 2H), 7.09 (t,

$J = 7.0$ Hz, 2H), 6.90 (t, $J = 8.0$ Hz, 2H), 5.88 (d, $J = 8.0$ Hz, 2H). Anal. Calcd for $C_{38}H_{22}F_{12}IrN_4PS_2$: C, 43.47; H, 2.11; N, 5.34. Found: C, 43.52; H, 2.28; N, 5.10%. FAB-mass (m/e): found, 613 $[M - \text{bpyCF}_3 - \text{PF}_6^-]^+$; 905 $[M - \text{PF}_6^-]^+$.

Phosphorescence Spectra and Quantum Yield Measurements. For room-temperature phosphorescence spectra and absolute emission quantum yield measurements, solutions were prepared in spectroscopic-grade CH_3CN (Dotite Spectrosol) with optical density below 0.2 at the selected excitation wavelength. Prior to each measurement, the sample solution was placed into a quartz cuvette (Hamamatsu Photonics A10095-02, 10×10 mm), and argon was bubbled through the solution for 20 min. Phosphorescence quantum yields and phosphorescence spectra were obtained on an absolute photoluminescence (PL) quantum yield spectrometer (Hamamatsu Photonics Quantaaurus-QY, C11347-01). This instrument consists of an integrating sphere, a monochromatized Xe arc lamp as the light source, a multichannel spectrometer, a back-thinned charge-coupled device (BT-CCD) detector, and a personal computer. Spectralon (Labsphere) is mounted on the internal surface of the integrating sphere as a high-reflectance material. An absolute method using the same system has recently been established and recognized as the most reliable method to determine emission quantum yields, as reported by Tobita, Nozaki, and co-workers including Hamamatsu Photonics K. K.³³ For low-temperature measurements, an EtOH–MeOH (1:1 v/v) mixture or 2-methyltetrahydrofuran (2-MeTHF) was chosen as a glass-forming solvent, and solutions were prepared with optical density of ca. 0.1 at the selected excitation wavelength. The sample solution was placed into a quartz sample tube (Hamamatsu Photonics A10095-04) and sealed with a rubber septum. Absolute emission quantum yields and phosphorescence spectra were measured at 77 K with an absolute PL quantum yield spectrometer (Hamamatsu Photonics Quantaaurus-QY, C11347-01) equipped with a dewar flask holder (Hamamatsu Photonics A11238-04).

Phosphorescence Lifetime Measurements. Solutions were prepared in spectroscopic-grade CH_3CN (Dotite Spectrosol) with optical density below 0.1 at the selected excitation wavelength. Prior to each measurement, the sample solution was placed into a quartz cuvette (Hamamatsu Photonics A10095-02, 10×10 mm), and argon was bubbled through the solution for 20 min. Phosphorescence lifetimes were measured on a compact fluorescence lifetime spectrometer (Hamamatsu Photonics Quantaaurus-Tau, C11367-01).

Cyclic Voltammetry. Acetonitrile was purchased from Kanto Chemical Co., Inc. and distilled over calcium hydride prior to use for the electrochemical measurement. Cyclic voltammetry (CV) was carried out in nitrogen-purged acetonitrile using a HOKUTO DENKO potentiostat/galvanostat HAB-151 equipped with a Run-Time Corporation X–Y Recorder (Voltam-REC). Tetrabutylammonium perchlorate (0.1 M) in acetonitrile was used as a supporting electrolyte. The conventional three-electrode configuration consisted of a platinum wire working electrode (length: 5 mm, diameter: 0.3 mm), a platinum wire auxiliary electrode, and a Ag/AgCl reference electrode.

Density Functional Theory Calculations. Calculations were carried out using the Gaussian 03 program package.³⁴ Geometry optimizations were performed on the ground state using the B3LYP functional together with the 6-31G basis set on C, H, N, O, F, and S atoms; the LANL2DZ basis set was used on the Ir atom. An effective core potential (ECP) replaced the inner core electrons of iridium, leaving the outer core $[(5s)^2(5p)^6]$ electrons and the $(5d)^6$ valence electrons of Ir(III).^{21,35} Triplet states were calculated at the spin-unrestricted B3LYP (UB3LYP) functional with a spin multiplicity of 3. Furthermore, frequency calculations were performed on all optimized structures to confirm that no imaginary frequencies were obtained. Time-dependent DFT (TD-DFT) calculations were performed at the optimized ground-state geometry of each Ir complex.

General Procedure for Photoinduced Electron-Transfer (PET) Reactions. A 3 mL solution of $\text{CH}_3\text{CN}-\text{H}_2\text{O}$ (1:1 v/v) containing TEOA (302 mM), a sensitizer (20.0 μM), and MVCl_2 (130 μM) was placed into a quartz cuvette (10×10 mm). Argon was bubbled through the solution for 20 min, and the cuvette was sealed

with a screw cap. The solution was then irradiated using a 500 W xenon arc lamp through cutoff filters (L-39 + B-46, 454 ± 52 nm). The $\text{MV}^{*\bullet}$ absorbance at 604 nm was monitored on a JASCO V-560 spectrometer, and the concentration of $\text{MV}^{*\bullet}$ was calculated using its molar extinction coefficient ($\epsilon = 12\,400 \text{ M}^{-1} \text{ cm}^{-1}$).²⁶

■ ASSOCIATED CONTENT

📄 Supporting Information

UV–vis absorption spectra of the btp and bpy ligands; photoluminescence excitation spectra and cyclic voltammograms of the Ir complexes; phosphorescence spectrum of $\text{Ir}(\text{btp})_2(\text{acac})$ in 2-MeTHF at 77 K; emission spectrum of complex **4** recorded in EtOH– CH_3OH (1:1 v/v) at 77 K; results of the TD-DFT calculations; MO distributions obtained from the DFT calculations; change in the concentration of $\text{MV}^{*\bullet}$ vs irradiation time for the PET reactions with Ir sensitizers **1** and **3**; absorption spectra before and after the PET reactions with Ir sensitizers **1** and **3**; photophysical properties of complexes **1–3** in $\text{CH}_3\text{CN}-\text{H}_2\text{O}$ (1:1 v/v) at room temperature; Stern–Volmer plots; FAB-mass spectra of the Ir complexes. This material is available free of charge via the Internet at <http://pubs.acs.org>

■ AUTHOR INFORMATION

Corresponding Authors

*E-mail: ctaki@mail.ecc.u-tokyo.ac.jp (S.T.).

*E-mail: cmura@mail.ecc.u-tokyo.ac.jp (S.M.).

Notes

The authors declare no competing financial interest.

■ ACKNOWLEDGMENTS

We are grateful to Dr. Atsushi Okazawa (The University of Tokyo) for helpful discussions on the DFT calculation. In addition, we would like to thank Ryoto Kano (Kitasato University) for synthesis of 4,4'-bis(trifluoromethyl)-2,2'-bipyridyl.

■ REFERENCES

- (1) (a) Lowry, M. S.; Goldsmith, J. I.; Slinker, J. D.; Rohl, R.; Pascal, R. A., Jr.; Malliaras, G. G.; Bernhard, S. *Chem. Mater.* **2005**, *17*, 5712–5719. (b) Tamayo, A. B.; Garon, S.; Sajoto, T.; Djurovich, P. I.; Tsyba, I. M.; Bau, R.; Thompson, M. E. *Inorg. Chem.* **2005**, *44*, 8723–8732. (c) Nazeeruddin, Md. K.; Wegh, R. T.; Zhou, Z.; Klein, C.; Wang, Q.; De Angelis, F.; Fantacci, S.; Gratzel, M. *Inorg. Chem.* **2006**, *45*, 9245–9250. (d) Rothe, C.; Chiang, C.-J.; Jankus, V.; Abdullah, K.; Zeng, X.; Jitchati, R.; Batsanov, A. S.; Bryce, M. R.; Monkman, A. P. *Adv. Funct. Mater.* **2009**, *19*, 2038–2044. (e) Costa, R. D.; Ortí, E.; Bolink, H. J.; Graber, S.; Schaffner, S.; Neuburger, M.; Housecroft, C. E.; Constable, E. C. *Adv. Funct. Mater.* **2009**, *19*, 3456–3463.
- (2) (a) Leung, S.-K.; Kwok, K. Y.; Zhang, K. Y.; Lo, K. K.-W. *Inorg. Chem.* **2010**, *49*, 4984–4995. (b) Zhao, Q.; Huang, C.; Li, F. *Chem. Soc. Rev.* **2011**, *40*, 2508–2524. (c) You, Y. *Curr. Opin. Chem. Biol.* **2013**, *17*, 699–707.
- (3) (a) Lowry, M. S.; Bernhard, S. *Chem.—Eur. J.* **2006**, *12*, 7970–7977. (b) Ladouceur, S.; Zysman-Colman, E. *Eur. J. Inorg. Chem.* **2013**, 2985–3007.
- (4) (a) Takizawa, S.; Aboshi, R.; Murata, S. *Photochem. Photobiol. Sci.* **2011**, *10*, 895–903. (b) Sun, J.; Zhao, J.; Guo, H.; Wu, W. *Chem. Commun.* **2012**, *48*, 4169–4171. (c) Hallett, A. J.; White, N.; Wu, W.; Cui, X.; Horton, P. N.; Coles, S. J.; Zhao, J.; Pope, S. J. A. *Chem. Commun.* **2012**, *48*, 10838–10840. (d) Jin, J.; Shin, H.-W.; Park, J. H.; Park, J. H.; Kim, E.; Ahn, T. K.; Ryu, D. H.; Son, S. U. *Organometallics* **2013**, *32*, 3954–3959. (e) Iqbal, N.; Choi, S.; You, Y.; Cho, E. J. *Tetrahedron Lett.* **2013**, *54*, 6222–6225.

- (5) Lalevée, J.; Dumur, F.; Mayer, C. R.; Gignes, D.; Nasr, G.; Tehfe, M.-A.; Telitel, S.; Morlet-Savary, F.; Graff, B.; Fouassier, J. P. *Macromolecules* **2012**, *45*, 4134–4141.
- (6) (a) Narayanam, J. M. R.; Stephenson, C. R. J. *Chem. Soc. Rev.* **2011**, *40*, 102–113. (b) Prier, C. K.; Rankic, D. A.; MacMillan, D. W. C. *Chem. Rev.* **2013**, *113*, 5322–5363.
- (7) (a) Goldsmith, J. I.; Hudson, W. R.; Lowry, M. S.; Anderson, T. H.; Bernhard, S. *J. Am. Chem. Soc.* **2005**, *127*, 7502–7510. (b) Tinker, L. L.; McDaniel, N. D.; Curtin, P. N.; Smith, C. K.; Ireland, M. J.; Bernhard, S. *Chem.—Eur. J.* **2007**, *13*, 8726–8732.
- (8) (a) Fihri, A.; Artero, V.; Pereira, A.; Fontecave, M. *Dalton Trans.* **2008**, 5567–5569. (b) Gartner, F.; Sundararaju, B.; Surkus, A.-E.; Boddien, A.; Loges, B.; Junge, H.; Dixneuf, P. H.; Beller, M. *Angew. Chem., Int. Ed.* **2009**, *48*, 9962–9965. (c) Gartner, F.; Cozzula, D.; Losse, S.; Boddien, A.; Anilkumar, G.; Junge, H.; Schulz, T.; Marquet, N.; Spannenberg, A.; Gladiali, S.; Beller, M. *Chem.—Eur. J.* **2011**, *17*, 6998–7006. (d) Zhang, P.; Wang, M.; Na, Y.; Li, X.; Jiang, Y.; Sun, L. *Dalton Trans.* **2010**, 39, 1204–1206. (e) Jasimuddin, S.; Yamada, T.; Fukuju, K.; Otsuki, J.; Sakai, K. *Chem. Commun.* **2010**, 46, 8466–8468. (f) Zhang, P.; Jacques, P.-A.; Chavarot-Kerlidou, M.; Wang, M.; Sun, L.; Fontecave, M.; Artero, V. *Inorg. Chem.* **2012**, *51*, 2115–2120. (g) Cui, H.-H.; Hu, M.-Q.; Wen, H.-M.; Chai, G.-L.; Ma, C.-B.; Chen, H.; Chen, C.-N. *Dalton Trans.* **2012**, 41, 13899–13907. (h) Whang, D. R.; Sakai, K.; Park, S. Y. *Angew. Chem., Int. Ed.* **2013**, *52*, 11612–11615.
- (9) (a) Yuan, Y.-J.; Zhang, J.-Y.; Yu, Z.-T.; Feng, J.-Y.; Luo, W.-J.; Ye, J.-H.; Zou, Z.-G. *Inorg. Chem.* **2012**, *51*, 4123–4133. (b) Takizawa, S.; Pérez-Bolívar, C.; Anzenbacher, P., Jr.; Murata, S. *Eur. J. Inorg. Chem.* **2012**, 3975–3979.
- (10) (a) Lamansky, S.; Djurovich, P.; Murphy, D.; Abdel-Razzaq, F.; Lee, H.-E.; Adachi, C.; Burrows, P. E.; Forrest, S. R.; Thompson, M. E. *J. Am. Chem. Soc.* **2001**, *123*, 4304–4312. (b) Finkenzeller, W. J.; Hofbeck, T.; Thompson, M. E.; Yersin, H. *Inorg. Chem.* **2007**, *46*, 5076–5083. (c) Zhao, Q.; Cao, T.; Li, F.; Li, X.; Jing, H.; Yi, T.; Huang, C. *Organometallics* **2007**, *26*, 2077–2081. (d) Zhang, S.; Hosaka, M.; Yoshihara, T.; Negishi, K.; Iida, Y.; Tobita, S.; Takeuchi, T. *Cancer Res.* **2010**, *70*, 4490–4498. (e) Murase, T.; Yoshihara, T.; Tobita, S. *Chem. Lett.* **2013**, *41*, 262–263.
- (11) (a) Adachi, C.; Baldo, M. A.; Forrest, S. R.; Lamansky, S.; Thompson, M. E.; Kwong, R. C. *Appl. Phys. Lett.* **2001**, *78*, 1622–1624. (b) Kawamura, Y.; Goushi, K.; Brooks, J.; Brown, J. J.; Sasabe, H.; Adachi, C. *Appl. Phys. Lett.* **2005**, *86*, 071104. (c) Bae, H. J.; Chung, J.; Kim, H.; Park, J.; Lee, K. M.; Koh, T.-W.; Lee, Y. S.; Yoo, S.; Do, Y.; Lee, M. H. *Inorg. Chem.* **2014**, *53*, 128–138.
- (12) (a) Li, Y.; Liu, Y.; Zhou, M. *Dalton Trans.* **2012**, 41, 3807–3816. (b) Woo, H.; Cho, S.; Han, Y.; Chae, W.-S.; You, Y.; Nam, W. *J. Am. Chem. Soc.* **2013**, *135*, 4771–4787.
- (13) (a) Guerrero-Martinez, A.; Vida, Y.; Dominguez-Gutierrez, D.; Albuquerque, R. Q.; De Cola, L. *Inorg. Chem.* **2008**, *47*, 9131–9133. (b) Kiran, R. V.; Hogan, C. F.; James, B. D.; Wilson, D. J. D. *Eur. J. Inorg. Chem.* **2011**, 4816–4825.
- (14) Li, C.; Yu, M.; Sun, Y.; Wu, Y.; Huang, C.; Li, F. *J. Am. Chem. Soc.* **2011**, *133*, 11231–11239.
- (15) Blanton, C. B.; Murtaza, Z.; Shaver, R. J.; Rillema, D. P. *Inorg. Chem.* **1992**, *31*, 3230–3235.
- (16) (a) Caspar, J. V.; Meyer, T. J. *Inorg. Chem.* **1983**, *22*, 2444–2453. (b) Wilson, J. S.; Chawdhury, N.; Al-Mandhary, M. R. A.; Younus, M.; Khan, M. S.; Raithby, P. R.; Kohler, A.; Friend, R. H. *J. Am. Chem. Soc.* **2001**, *123*, 9412–9417.
- (17) (a) Karatsu, T.; Nakamura, T.; Yagai, S.; Kitamura, A.; Yamaguchi, K.; Matsushima, Y.; Iwata, T.; Hori, Y.; Hagiwara, T. *Chem. Lett.* **2003**, *32*, 886–887. (b) Treboux, G.; Mizukami, J.; Yabe, M.; Nakamura, S. *Chem. Lett.* **2007**, *36*, 1344–1345. (c) Abrahamsson, M.; Lundqvist, M. J.; Wolpher, H.; Johansson, O.; Eriksson, L.; Bergquist, J.; Rasmussen, T.; Becker, H.-C.; Hammarström, L.; Norrby, P.-O.; Åkermark, B.; Persson, P. *Inorg. Chem.* **2008**, *47*, 3540–3548. (d) Sajoto, T.; Djurovich, P. I.; Tamayo, A. B.; Oxgaard, J.; Goddard, W. A., III; Thompson, M. E. *J. Am. Chem. Soc.* **2009**, *131*, 9813–9822. (e) Wagenknecht, P. S.; Ford, P. C. *Coord. Chem. Rev.* **2011**, *255*, 591–616. (f) Brown, D. G.; Sanguantrakun, N.; Schulze, B.; Schubert, U. S.; Berlinguette, C. P. *J. Am. Chem. Soc.* **2012**, *134*, 12354–12357. (g) Breivogel, A.; Meister, M.; Forster, C.; Laquai, F.; Heinze, K. *Chem.—Eur. J.* **2013**, *19*, 13745–13760.
- (18) (a) Casper, J. V.; Meyer, T. J. *J. Am. Chem. Soc.* **1983**, *105*, 5583–5590. (b) Osterman, T.; Abrahamsson, M.; Becker, H.-C.; Hammarstrom, L.; Persson, P. *J. Phys. Chem. A* **2012**, *116*, 1041–1050. (c) Monti, F.; Kessler, F.; Delgado, M.; Frey, J.; Bazzanini, F.; Accorsi, G.; Armaroli, N.; Bolink, H. J.; Ortí, E.; Scopelliti, R.; Nazeeruddin, M. K.; Baranoff, E. *Inorg. Chem.* **2013**, *52*, 10292–10305.
- (19) (a) Tsuboyama, A.; Iwawaki, H.; Furugori, M.; Mukaide, T.; Kamatani, J.; Igawa, S.; Moriyama, T.; Miura, S.; Takiguchi, T.; Okada, S.; Hoshino, M.; Ueno, K. *J. Am. Chem. Soc.* **2003**, *125*, 12971–12979. (b) Chiridon, D. N.; McCusker, C. E.; Castellano, F. N.; Bernhard, S. *Inorg. Chem.* **2013**, *52*, 8795–8904.
- (20) We thank one of the reviewers who suggested 2-MeTHF as a solvent of choice for an additional attempt to obtain the phosphorescence spectrum of complex 4 at 77 K.
- (21) Hay, P. J. *J. Phys. Chem. A* **2002**, *106*, 1634–1641.
- (22) (a) Nozaki, K. *J. Chin. Chem. Soc.* **2006**, *53*, 101–112. (b) Dragonetti, C.; Falciola, L.; Mussini, P.; Righetto, S.; Roberto, D.; Ugo, R.; Valore, A. *Inorg. Chem.* **2007**, *46*, 8533–8547. (c) Yang, L.; Okuda, F.; Kobayashi, K.; Nozaki, K.; Tanabe, Y.; Ishii, Y.; Haga, M. *Inorg. Chem.* **2008**, *47*, 7154–7165. (d) Costa, R. D.; Monti, F.; Accorsi, G.; Barbieri, A.; Bolink, H. J.; Ortí, E.; Armaroli, N. *Inorg. Chem.* **2011**, *50*, 7229–7238. (e) Ladouceur, S.; Fortin, D.; Zysman-Colman, E. *Inorg. Chem.* **2011**, *50*, 11514–11526. (f) Li, X.-N.; Wu, Z.-J.; Li, X.-Y.; Zhang, H.-J.; Liu, X.-J. *J. Comput. Chem.* **2011**, *32*, 1033–1042. (g) Shan, G.-G.; Li, H.-B.; Sun, H.-Z.; Cao, H.-T.; Zhu, D.-X.; Su, Z.-M. *Dalton Trans.* **2013**, 42, 11056–11065.
- (23) Kasha, M. *Discuss. Faraday Soc.* **1950**, *9*, 14–19.
- (24) (a) Yeh, Y.-S.; Cheng, Y.-M.; Chou, P.-T.; Lee, G.-H.; Yang, C.-H.; Chi, Y.; Shu, C.-F.; Wang, C.-H. *ChemPhysChem* **2006**, *7*, 2294–2297. (b) Park, G. Y.; Kim, Y. S.; Ha, Y. *Curr. Appl. Phys.* **2007**, *7*, 390–395. (c) Glazer, E. C.; Magde, D.; Tor, Y. *J. Am. Chem. Soc.* **2007**, *129*, 8544–8551. (d) Lo, K. K.-W.; Zhang, K. Y.; Leung, S.-K.; Tang, M.-C. *Angew. Chem., Int. Ed.* **2008**, *47*, 2213–2216. (e) You, Y.; Han, Y.; Lee, Y.-M.; Park, S. Y.; Nam, W.; Lippard, S. J. *J. Am. Chem. Soc.* **2011**, *133*, 11488–11491. (f) Ladouceur, S.; Donato, L.; Romain, M.; Mudraboyina, B. P.; Johansen, M. B.; Wisner, J. A.; Zysman-Colman, E. *Dalton Trans.* **2013**, 42, 8838–8847.
- (25) Lowry, M. S.; Hudson, W. R.; Pascal, R. A., Jr.; Bernhard, S. *J. Am. Chem. Soc.* **2004**, *126*, 14129–14135.
- (26) Mizushima, T.; Yoshida, A.; Harada, A.; Yoneda, Y.; Minatani, T.; Murata, S. *Org. Biomol. Chem.* **2006**, *4*, 4336–4344.
- (27) (a) Kirch, M.; Lehn, J.-M.; Sauvage, J.-P. *Helv. Chim. Acta* **1979**, *62*, 1345–1384. (b) Borgarello, E.; Kiwi, J.; Pelizzetti, E.; Visca, M.; Gratzel, M. *J. Am. Chem. Soc.* **1981**, *103*, 6324–6329. (c) Yamauchi, K.; Masaoka, S.; Sakai, K. *J. Am. Chem. Soc.* **2009**, *131*, 8404–8406. (d) Ogawa, M.; Ajayakumar, G.; Masaoka, S.; Kraatz, H.-B.; Sakai, K. *Chem.—Eur. J.* **2011**, *17*, 1148–1162. (e) Watanabe, K.; Takizawa, S.; Murata, S. *Chem. Lett.* **2011**, *40*, 345–347. (f) Watanabe, K.; Moriya, K.; Kouyama, T.; Onoda, A.; Minatani, T.; Takizawa, S.; Murata, S. *J. Photochem. Photobiol. A* **2011**, *221*, 113–122.
- (28) Murov, S. L.; Carmichael, I.; Hug, G. L. *Handbook of Photochemistry*, 2nd ed.; Marcel Dekker, Inc.: New York, 1993.
- (29) Fujii, S.; Morita, T.; Kimura, S. *Langmuir* **2008**, *24*, 5608–5614.
- (30) Sajoto, T.; Djurovich, P. I.; Tamayo, A.; Yousufuddin, M.; Bau, R.; Thompson, M. E.; Holmes, R. J.; Forrest, S. R. *Inorg. Chem.* **2005**, *44*, 7992–8003.
- (31) Holmes, R. J.; Forrest, S. R.; Sajoto, T.; Tamayo, A.; Djurovich, P. I.; Thompson, M. E.; Brooks, J.; Tung, Y.-J.; D’Andrade, B. W.; Weaver, M. S.; Kwong, R. C.; Brown, J. J. *Appl. Phys. Lett.* **2005**, *87*, 243507.
- (32) Furue, M.; Maruyama, K.; Oguni, T.; Naiki, M.; Kamachi, M. *Inorg. Chem.* **1992**, *31*, 3792–3795.
- (33) (a) Suzuki, K.; Kobayashi, A.; Kaneko, S.; Takehira, K.; Yoshihara, T.; Ishida, H.; Shiina, Y.; Oishi, S.; Tobita, S. *Phys. Chem. Chem. Phys.* **2009**, *11*, 9850–9860. (b) Kobayashi, A.; Suzuki, K.

Yoshihara, T.; Tobita, S. *Chem. Lett.* **2010**, *39*, 282–283. (c) Ishida, H.; Tobita, S.; Hasegawa, Y.; Katoh, R.; Nozaki, K. *Coord. Chem. Rev.* **2010**, *254*, 2449–2458.

(34) Frisch, M. J.; Trucks, G. W.; Schlegel, H. B.; Scuseria, G. E.; Robb, M. A.; Cheeseman, J. R.; Montgomery, Jr., J. A.; Vreven, T.; Kudin, K. N.; Burant, J. C.; Millam, J. M.; Iyengar, S. S.; Tomasi, J.; Barone, V.; Mennucci, B.; Cossi, M.; Scalmani, G.; Rega, N.; Petersson, G. A.; Nakatsuji, H.; Hada, M.; Ehara, M.; Toyota, K.; Fukuda, R.; Hasegawa, J.; Ishida, M.; Nakajima, T.; Honda, Y.; Kitao, O.; Nakai, H.; Klene, M.; Li, X.; Knox, J. E.; Hratchian, H. P.; Cross, J. B.; Adamo, C.; Jaramillo, J.; Gomperts, R.; Stratmann, R. E.; Yazyev, O.; Austin, A. J.; Cammi, R.; Pomelli, C.; Ochterski, J. W.; Ayala, P. Y.; Morokuma, K.; Voth, G. A.; Salvador, P.; Dannenberg, J. J.; Zakrzewski, V. G.; Dapprich, S.; Daniels, A. D.; Strain, M. C.; Farkas, O.; Malick, D. K.; Rabuck, A. D.; Raghavachari, K.; Foresman, J. B.; Ortiz, J. V.; Cui, Q.; Baboul, A. G.; Clifford, S.; Cioslowski, J.; Stefanov, B. B.; Liu, G.; Liashenko, A.; Piskorz, P.; Komaromi, I.; Martin, R. L.; Fox, D. J.; Keith, T.; Al-Laham, M. A.; Peng, C. Y.; Nanayakkara, A.; Challacombe, M.; Gill, P. M. W.; Johnson, B.; Chen, W.; Wong, M. W.; Gonzalez, C.; Pople, J. A. *Gaussian 03*, Revision C.02; Gaussian, Inc., Wallingford, CT, 2004.

(35) Hay, P. J.; Wadt, W. R. *J. Chem. Phys.* **1985**, *82*, 270–283.